The metabolic cost of flagellar motion in *Pseudomonas putida* KT2440

by

Esteban Martínez-García, Pablo I. Nikel, Max Chavarría[&], and Víctor de Lorenzo[*]

[1]Systems Biology Program, Centro Nacional de Biotecnología-CSIC, Campus de Cantoblanco, 28049, Madrid (Spain);

Keywords: *Pseudomonas putida,* flagella, reducing power, stress resistance, metabolic robustness, trade-off

Running Title: Cost *vs* benefit of *P. putida*'s flagella

---

* Correspondence to: Víctor de Lorenzo
Centro Nacional de Biotecnología-CSIC
Campus de Cantoblanco, Madrid 28049, Spain
Tel.: 34- 91 585 45 36; Fax: 34-91 585 45 06
E-mail: vdlorenzo@cnb.csic.es

[&] Current address: Escuela de Química, Universidad de Costa Rica, 2060 San José, Costa Rica

Summary

Although the flagellar machinery of environmental bacteria endows cells with a phenomenal survival device, it also consumes much of the metabolic currency necessary for fuelling such a vigorous nano-motor. The physiological cost of flagella-related functions of the soil bacterium *Pseudomonas putida* KT2440 was examined and quantified through the deletion of a ~70-kb DNA segment of the genome (~1.1%), which includes relevant structural and regulatory genes in this microorganism. The resulting strain lacked the protruding polar cords that define flagella in the wild-type *P. putida* strain and was unable of any swimming motility while showing a significant change in surface hydrophobicity. However, these deficiencies were otherwise concomitant with clear physiological advantages: rapid adaptation of the deleted strain to both glycolytic and gluconeogenic carbon sources, increased energy charge and, most remarkably, improved tolerance to oxidative stress, reflecting an increased NAD(P)H/NAD(P)$^+$ ratio. These qualities improve the endurance of non-flagellated cells to the metabolic fatigue associated with rapid growth in rich medium. Thus, flagellar motility represents the archetypal trade-off involved in acquiring environmental advantages at the cost of a considerable metabolic burden.

Introduction

Motility is an important quality of many bacteria for exploring the environment for nutrients, escaping from predator grazing and moving away from detrimental physicochemical conditions. The rotation of the flagella, an external long helical filament, thrusts bacteria through liquid media and wet surfaces. Self-propulsion is well-conserved among microorganisms, where almost two-thirds of sequenced bacteria are motile (Wei *et al.,* 2011). While there are several types of bacterial motility, swimming in liquid media and swarming on wet surfaces are both flagella-dependent motions. Flagella also play a key role in adhesion, biofilm formation, root colonisation and host invasion (Kirov 2003). The bacterial flagellum is a filament propeller with a rotary motor and an export apparatus. Depending on the bacterial species, flagella vary in number and position within the cell, from polar to peritrichous (distributed around cell surface). More than 50 genes are typically involved in flagella production, a complex process that requires coordination in space and time (Liu and Ochman 2007). To this end, the promoters of flagellar regulons are hierarchically organised into different classes, which are temporally regulated through the assemblage (Dasgupta *et al.,* 2003).

Movement toward either oxygen (aerotaxis: Bibikov *et al.,* 1997; Rebbapragada *et al.,* 1997) or nutrients and away from repellents (chemotaxis: Bren and Eisenbach 2000) directs flagella motion. The rotation of the filaments is powered through the proton motive force (PMF) and not ATP (Larsen *et al.,* 1974; Berg 2003). In *Escherichia coli*, the rotation frequency is greater than 100 Hz (Lowe *et al.,* 1987), generating speed velocities of approximately 25 μm s^{-1} (Macnab 1996). In the same bacterium, the flagellar filaments rotate either counterclockwise (CCW) or clockwise (CW). For CCW motion, the left-handed helical flagellar structure is assembled in bundles and propels the cell in a pushing motion. CW rotation produces tumbling, causing the cell to move without a defined orientation (Macnab 1977). However, in *Pseudomonas putida*, unlike *E. coli*, the flagella rotate equally CCW or CW and also have a pause mode generating run-reverse-run trajectories (Qian *et al.,* 2013). Both the production and the rotation of flagella are energy-demanding processes for the cell. In *E. coli*, flagellar synthesis imposes a cost of approximately 2% of the biosynthetic energy expenditure of the cell, while rotation of the cords demands ~0.1% of the total energy cost (Macnab 1996). Although flagella are important structures for coping with environmental circumstances, under certain conditions, such as laboratory settings, not having this organelle could provide the bacteria with more energy and/or reducing power. Thus, non-flagellated cells would be expected to allocate these resources to improve endurance under stress. Trade-offs, in which a beneficial change in one trait imposes a negative variation in another aspect, are common in Nature. Several studies have shown that in the laboratory, where the expression of flagella is not crucial for survival, losing this appendage and its imposed metabolic burden benefit bacteria (Macnab 1996; Jishage and Ishihama 1997). In addition, directed deletions of *fliA* (encoding the sigma factor F) in *E. coli* are beneficial in a number of traits as well (Fontaine *et al.,* 2008).

In the present study, we have inspected and quantified the metabolic burden associated with flagellar assembly and motion in the environmental bacterium *P. putida* KT2440, a non-pathogenic microorganism commonly found in water, soil and in the rhizosphere as a plant and root-associated partner (Dos Santos *et al.,* 2004). This bacterium is endowed with a broad metabolic capacity and it is responsible for the oxidation of a wide variety of toxic organic compounds, making *P. putida* KT2440 a choice model for biotechnological applications (Nelson *et al.,* 2002; Pieper *et al.,* 2004). *P. putida* is a multi-flagellated species, having five to seven flagella at one pole (Harwood *et al.,* 1989). Although flagella-less *P. putida* strains are available (Graf and Altenbuchner 2011), we set out to inspect the

emergent properties of a strain entirely lacking the whole of the corresponding genes. The rationale is that comparison of the performance of isogenic flagella-plus and flagella-minus bacteria in a range of physicochemical scenarios should enable the measurement of the metabolic burden associated with this motility engine. The results below not only reveal a suite of evolutionary trade-offs between metabolic strength and motion, but also suggest ways to improve the value of *P. putida* as a model bacterium of biotechnological interest.

Results and Discussion

Identifying and deleting flagella-related genes in the genome of P. putida KT2440

In order to examine the interplay between motion and metabolism in *P. putida* KT2440, we first inspected its genome for genes involved in flagellar synthesis and functioning (Dos Santos *et al.,* 2004). This survey exposed a region spanning from PP4329 to PP4397, comprising a total of 69 genes, which included elements for flagellar export and assembly, the regulatory elements and several chemotaxis genes (Fig. 1A, 1B, and Supplementary Table S1). Notably, outside this large operon, there are two extra copies of the stator genes *motA* (PP4905) and *motB* (PP4904), similar to those found in the *P. aeruginosa* genome (Toutain *et al.,* 2005). Three genes of the flagellar operon encode putative enzymes (i.e. one cystathionine β-lyase, one aminotransferase, and one β-ketoacyl/acyl-carrier-protein synthase) along with six genes encoding hypothetical proteins with unknown functions (Supplementary Table S1). We then deleted the region spanning from PP4329 to PP4397, representing ~1.1% of the KT2440 genome, using the I-SceI technology described in Martinez-Garcia and de Lorenzo (2011). The deletion was genetically confirmed through PCR amplification of the TS1-TS2 intervening region and by the absence of any amplification of two genes located within the flagellar operon (PP4335 and PP4352; Fig. 1C). We also sequenced the junction of the deleted strain to confirm the absence of mutations in the genomic region left after the deletion. The results confirmed the sole, precise deletion of the operon of interest in the resulting strain.

Motility and morphological analyses

Bacteria use flagella predominantly to move through the environment. We tested the swimming capabilities of the deleted strain compared with that of the wild-type strain on M9 minimal medium with 0.3% (w/v) agar supplemented with glucose, succinate and fructose as the sole carbon (C) source. The cells were spotted onto the surface, and their swimming halo was evaluated after 48 h. The mutant strain was unable to swim on any of the media tested, regardless of the C source. The results of a representative experiment on M9 medium containing succinate are shown in Fig. 2A; the other swimming experiments are shown in the Supplementary Fig. S1. To confirmed that the lack of swimming in the mutant strain resulted from the complete elimination of flagellar synthesis and not from cells with non-motile cords we verified the complete absence of the filaments using transmission electron microscopy after negative staining. While several cords were observed in the wild type strain (Fig. 2B), the deleted strain (Fig. 2C and 2D) completely lacked any of them protruding from the surface.

Sedimentation and surface hydrophobicity

In the laboratory, where cultures are routinely shaken, the loss of flagella is not detrimental for non-motile cells. However, when in static ecosystems flagella are needed for chemotaxis (Bren and Eisenbach 2000) and aerotaxis (Bibikov *et al.,* 1997; Rebbapragada *et al.,* 1997). To simulate a static environment, we incubated a cell-saturated culture without shaking for 24 h. The results showed that non-flagellated cells sediment faster than wild type cells, as shown in Fig. 3A. Thus, for *P. putida* KT2440 (a strict aerobe), losing the ability to position itself within an oxygen gradient may have an important environmental cost. Since flagellar filaments are located on the outer membrane, we also determined whether lacking these structures affected the hydrophobicity of the cell surface using the microbial adherence to hydrocarbon (MATH) test (Rosenberg *et al.,* 1980; Rosenberg 1984), as described in Experimental procedures. This technique is based on the different levels of attachment to hexadecane depending on the surface hydrophobicity of the cells. We observed that the mutant strain has a less hydrophobic surface (MATH score 36.4 ± 11.5) than the wild type strain (59.3 ± 12.1, $P < 0.0001$, *t*-test; Fig. 3B), potentially affecting the interaction of this strain with the surrounding environment.

Non-flagellated cells form more biofilm than wild-type cells

Most bacteria are social organisms commonly found as biofilms in nature (Hall-Stoodley *et al.,* 2004; Kolter and Greenberg 2006). Bacterial lifestyle, either motile or sessile, depends on flagellar activity and exopolysaccharide production as well as other matrix components (exopolymeric substance, EPS). In many bacteria, these phenomena are co-ordinated by the secondary messenger 3',5'-cyclic diguanylate (c-di-GMP; Simm *et al.,* 2004). Because the mutant strain does not actively move, we assessed the ability of this strain to establish a biofilm on abiotic surfaces at various times as shown in Fig. 4. In all cases it was noticeable that neither the wild type nor the mutant formed much biofilm in LB (Fig. 4) as compared to minimal medium with a defined C source. We thus limited our analyses to biofilms formed in synthetic media as follows. First, inspection of plates at 5 h revealed that the wild-type strain adhered to surfaces more than non-flagellated cells in all media tested (Fig. 4A). This result is consistent with the known role of flagella in the early steps of biofilm formation (Pratt and Kolter 1998). Second, by 24 h, the mutant strain formed more biofilm than the wild type strain in all the media tested (Fig. 4B). One explanation to this somewhat paradoxical behaviour is that –similarly to *P. aeruginosa,* the loss of the flagellar operon could de-repress EPS production (Hickman and Harwood 2008). To examine this possibility we estimated EPS production of each of the strains through a dye-binding agar plate test. For this, 2 µl of overnight cultures of either strain were spotted on tryptone agar plates containing a mixture of Congo red and Coomassie brilliant blue (see Experimental procedures) and incubated at room temperature for 24 h. As binding these dyes is directly proportional to EPS production (Romling *et al.,* 1998; Friedman and Kolter 2004) this method allows to determine easily the relative levels the polymer. As shown in Fig. 4C, the non-flagellated cells formed smooth colonies, similar to wild type cells. However, the same cells bound more red dye than the parental strain, indicating that the flagella-less cells had produced more EPS what suffices to explain the increased biofilm formation observed. We also tested whether enhanced EPS included production of a cellulose-like polymer by comparing the ability of both strains to bind to calcofluor white in LB agar plates (Hansen *et al.,* 2007). In this case we did not observe any difference, suggesting that cellulose did not contribute to increasing EPS in the non-flagelated cells. Finally, we looked at persistence of the biofilms formed by non-motile cells once nutrients had been depleted upon prolonged incubation of the microtiter plates. Typically, up-regulation of flagella when cells starve is key for initiating a new planktonic cycle (Sauer *et al.,* 2004). As shown in Fig. 4D, the non-flagellated strain remained predominantly adhered to the surface of the plates after four days of incubation, probably due to the inability of cells to swim away from the biofilm. In contrast, the wild-type cells detached entirely from the surface during the same period of time.

Flagella influences lag phase when growing on different C sources

After documenting the gross phenotypes described above, we compared the physiology of the flagella-plus and flagella-minus strains. To evaluate the overall effect of lacking motion in the cellular physiology, we followed the growth profiles of the strains of interest in nutrient-rich (LB) and minimal medium (M9) containing gluconeogenic (succinate) and glycolytic (glucose and fructose) C sources (Fig. 5). The growth rate of the mutant strain was significantly lower than that of the wild type counterpart in LB (P = 0.0001, t-test). Marginally lower growth rates were observed on M9 plus succinate (P = 0.5, t-test) or glucose (P = 0.2, t-test). This result could partially reflect the increased sedimentation of the non-flagellated strain (see above) in the 96-well plates, where shaking conditions might not be optimal for proper growth. However, when fructose was used as a C source, contrasting results were observed, as the deleted strain grew faster compared with the wild type strain (P = 0.03, t-test). Interestingly, in all the media tested, the mutant strain grew earlier, the shortened lag phase being more evident on fructose (< 0.1 h for the Δflagella strain) compared with the wild-type strain (4.3 ± 0.6 h). In *P. putida*, fructose transport and phosphorylation are mediated through a sugar-specific PTS system comprising FruB (EI-HPr-EIIA) and FruA (EIIBC; Chavarria *et al.,* 2012). This hexose is subsequently catabolised through the Entner-Doudoroff, pentose phosphate and (incomplete) Embden-Meyerhof-Parnas pathways. These data suggest that the conversion of fructose into the intermediates that feed central metabolic pathways is more efficient in the non-flagellated strain, exposing a distinct distribution of metabolic fluxes. Thus, the deleted strain thrived more effectively than the wild type on different C sources, which prompted further investigation into the metabolic and physiological reasons for this growth advantage.

Phenotypic characterisation using PM technology

To obtain a global view of the physiological consequences of not having flagella, we performed phenotypic profiling using Biolog PM technology (Bochner *et al.,* 2001; Bochner 2009). We used plates PM1 to PM20 (see Supplemental Material) to examine different carbon, nitrogen, phosphorous and sulphur sources and to determine the effect of nutrient supplements, osmolytes, pH values and a broad chemical sensitivity panel. Altogether, this platform facilitated the examination of > 1000 different physiological conditions. The complete image with consensus calls is presented in Supplementary Fig.

S2, and a summary list of the phenotypes affected by the absence of flagella is shown in Supplementary Table S2. The majority of changes involved loss of functions (26 out of 27). The mutant strain poorly utilised the amino acid alanine (D and L forms) as a sole C source. Similarly, the mutant failed to use L-valine, L-isoleucine and three peptides containing either amino acid as N sources. Moreover, non-flagellated cells were comparatively sensitive to acidic pH (below 6), inhibitors of membrane and cell wall formation, toxic anions and ionophores. To confirm some of the observed phenotypes, we compared the viability of the wild type and non-flagellated cells after exposure to β-lactam antibiotics and pH extremes. The cells from overnight cultures were serially diluted and plated onto agar plates containing the stressor. As indicated in Fig. 6 and Supplementary Fig. S3, the deleted strain showed an increased sensitivity to β-lactam antibiotics (piperacillin, carbenicillin and ampicillin) that disrupt the cell wall. Furthermore, the mutant was more sensitive to acidic pH than wild type cells. However, no effect on cell survival was observed when exposed to basic pH (Fig. 6).

Flagellar motion impacts energy status and reducing power availability

In enterobacteria, the flagellar motor is built from the inside out in a complex, multi-step assembly and export process. A key component of the transport apparatus, FliI, is highly similar to both the β subunit of the F_0F_1-ATPase and to the components of bacterial type III secretory systems. The FliI homologue in *P. putida* KT2440 is PP4366, annotated as a flagellum-specific ATP synthase. The assembly of the motor and the transport of its components to the bacterial surface is a high-energy process. However, the rotation of the flagella itself is propelled by the H^+ gradient across the membrane, and this activity modifies the proton-motive force that ultimately fosters ATP generation. Within this framework, we assessed the ATP, ADP and AMP content in wild-type and non-flagellated cells exponentially growing on glucose. The adenylate energy charge (AEC), a general descriptor of the energy status of the cells, was slightly, but significantly ($P < 0.05$, *t*-test), higher in the non-flagellated strain (Fig. 7A). Accordingly, the ATP/ADP ratio in the non-flagellated strain was 1.3-fold higher than that in wild type strain KT2440 ($P < 0.05$, *t*-test). As the ATP levels in these cells are tightly controlled, a difference of 30% could significantly impact cell function. Taken together, these results indicate that avoiding the expenditure needed for flagella assembly and motility significantly modified the energy status of the cells.

The redox status is also a physiological trait closely associated with the energy homeostasis of the cells. Primary anabolic processes, such as the biosynthesis of biomass building blocks, consume a considerable share of reducing power, primarily in the form of NADPH. We analysed the redox status of the strains in this study by measuring the content of NAD^+, NADH, $NADP^+$ and NADPH in glucose-grown cells, and the corresponding redox ratios were calculated (Fig. 7B). Although we did not detect any significant difference in the catabolic charge (reflected in the NADH/NAD^+ ratio) of the cells, the non-flagellated mutant had a 1.2-fold higher NADPH/$NADP^+$ ratio than did the wild type strain ($P < 0.05$, *t*-test). This parameter reflects enhanced anabolic capability in the non-flagellated bacteria, which helps explaining the growth properties of these cells. Since NADPH provides the reducing equivalents necessary to fuel biosynthetic reactions within the cells (Neidhardt *et al.,* 1990; Russell and Cook 1995), biochemical steps that produce building blocks for biomass are expected to be favoured in the Δflagella mutant. Moreover, NADPH is the metabolic currency that balances the redox potential needed to protect cells against oxidative stress (e.g., by helping to regenerate reduced glutathione (Mailloux *et al.,* 2011) (Chavarria *et al.,* 2013; Imlay 2013). As the differences in NADPH availability should in turn translate into variations in sensitivity to oxidative stress, we explored this issue as described below.

The trade-off between physicochemical stress and motility

Stressed cells require NADPH to counteract oxidative damage. Therefore, we determined whether the increased reducing power in non-flagellated strain could be translated into an enhanced resistance to oxidative stress. We assessed the ability of the deleted strain to cope with the oxidative stressors paraquat and diamide. Paraquat catalyses the formation of reactive oxygen species (ROS) and diminishes the NADPH cellular pool (Bus and Gibson 1984). Diamide is a thiol-oxidising agent that oxidises glutathione, thus affecting the redox state of the cytoplasm (Wax *et al.,* 1970). These two oxidative stressors were used as indicators of the amount of available reducing power in non-flagellated cells. Thus, we compared the growth of the cells (OD_{600}) with and without the specific stressors for 24 h and plotted the survival ratio (OD_{600} with the drug to OD_{600} without any stressor) along time to observe the immediate effect and to assess the gross cellular responses to these drugs. Fig. 8A shows the survival ratio when cells were exposed to paraquat in four different media (LB and M9 added with either succinate, glucose or fructose). The deleted strain survived better than the wild type strain when exposed to paraquat-induced oxidative damage. In LB, the survival ratio after 4 h for the wild type strain

was 0.6 ± 0.14 *vs.* a survival ratio of 0.93 ± 0.04 for the deleted strain. In M9 plus succinate, the survival ratios after 9 h were 0.08 ± 0.05 (wild type) vs. 0.38 ± 0.003 (non-flagellated); in M9 plus glucose, the survival ratios after 9 h were 0.04 ± 0.011 (wild type) *vs.* 0.16 ± 0.015 (non-flagellated); and in M9 fructose the survival ratios after 14 h were 0.1 ± 0.01 (wild type) *vs.* 0.3 ± 0.09 (non-flagellated). When treated with diamide (Fig. 8B), the non-flagellated cells showed better survival after exposure to the stressor in LB at 4 h, the survival ratio was 0.25 ± 0.02 for the wild type strain *vs.* 0.68 ± 0.04 for the non-flagellated strain; at 9 h in M9 plus glucose, the survival ratios were 0.04 ± 0.011 (wild type) vs. 0.32 ± 0.18 (non-flagellated); and in M9 plus fructose at 14 h the survival ratios were 0.21 ± 0.06 for the wild type strain *vs.* 0.68 ± 0.07 for the non-flagellated strain. In M9 plus succinate the survival ratios after 9 h were similar in both strains [0.22 ± 0.17 (wild type) vs. 0.19 ± 0.12 (non-flagellated)]. Resistance to these stressors was also verified using spotting assays, where the resistance to paraquat was more obvious in the non-flagellated strain than the resistance to diamide in these same cells (Fig. 6), thereby confirming the results of the liquid experiments and suggesting that the mutant strain had more reducing power available to quickly handle oxidative stressors. We also examined the resistance of non-flagellated cells to UV irradiation, as bacteria are commonly exposed to this type of stress in the environment. Because DNA repairing mechanisms consume also energy and reducing power, we speculated that the lack of flagella could be beneficial as well to increase endurance to such an insult. To look into this possibility, we compared the ability of the wild type and non-flagellated strains to survive UV exposure. Both strains were distributed onto an agar plate and subject to an irradiation gradient. As anticipated, the non-flagellated strain was able to resist higher doses of UV than the wild type strain (Fig. 6).

Improved viability of the non-flagellated strain in stationary phase

Because cells lacking flagella were able to cope with oxidative stresses better than the wild type strain, we determined whether this benefit improves stationary phase viability. We performed a viability test through staining with propidium iodide (PI) and measuring the proportion of PI-stained cells. PI is a fluorescent dye that only stains cells with damaged membranes, but does not pass through intact cell envelopes. This method is commonly used to distinguish between live and dead bacteria (Williams *et al.,* 1998). We used flow cytometry (as described in Experimental procedures) to quantify the percentage of PI-stained cells in overnight cultures grown in LB and M9 with glucose. Cultures of the mutant strain had

fewer dead cells (~1.4%) than those of the wild type (~4.7%) in LB ($P < 0.0001$, *t*-test; Fig. 9A), while there was no difference in viability when cells were grown in M9 plus glucose (Fig. 9B). The different number of PI-stained cells observed in LB was unrelated to the different surface hydrophobicity of the deleted strain, as this alteration was not observed in minimal medium. In addition, the reduced numbers observed in rich medium are consistent with data reported for *E. coli* (Fontaine *et al.,* 2008) showing that *fliA* mutants exhibited lower mortality than the wild type. The fewer number of dead cells for the non-flagellated strain might reflect the higher energy and reducing power of the mutant, which likely counteract the oxidative stress associated with rapid growth (Ackermann 2008). Moreover, the non-flagellated strain might not show an improvement in viability when cultured on M9 plus glucose because the pH of this media turns slightly acidic during cellular growth due to the generation of gluconate and 2-ketogluconate (del Castillo *et al.,* 2007). As demonstrated above, the deleted strain is relatively more sensitive to pH below 6, potentially disguising other beneficial effects conferred by the lack of flagellar synthesis.

Conclusion

To study the metabolic trade-offs of producing flagella, we deleted the major motility apparatus in the environmental bacterium *P. putida* KT2440. The non-flagellated strain did not swim on soft agar plates, rapidly sedimented in static environments and produced more biofilm than did the parental strain. In addition, the lack of flagellar synthesis affected the surface, which became less hydrophobic. Interestingly, the non-flagellated strain presented a shorter lag phase and was more resistant to oxidative stresses and UV exposure than the wild type strain. Thus, the lack of flagellar synthesis might confer a surplus of energy (ATP) and reducing power (NADPH) that the deleted strain could allocate for other functions. Taken together, these data suggest an environmental trade-off that favours motion at the expense of losing energy and reducing power, and thus motile cells become more sensitive to stress. Under laboratory conditions where nutrients are typically in excess and aeration can be manipulated at ease lacking flagella might be in fact an advantage. *P. putida* is increasingly becoming a relevant microbial cell factory for the synthesis of heterologous biomolecules as well as a relevant biocatalyst for biotransformations (Nikel 2012; Poblete-Castro *et al.,* 2012). Most of these industrially-relevant processes rely on high NADPH regeneration rates and call for biocatalysts highly resistant to stressful conditions (Blank *et al.,* 2008). Thus, manipulations that endow *P. putida* with increased energy charge

and enhanced NADPH availability -such as the ones described in this study, should be instrumental for the development of a robust microbial platform for biocatalysis.

Experimental procedures

Strains, plasmid, media and growth conditions

All bacterial strains and plasmids presented in this work are listed in Table 1. Cells were routinely grown on LB medium (10 g l^{-1} of tryptone, 5 g l^{-1} of yeast extract and 5 g l^{-1} of NaCl) at 30ºC for *P. putida* whereas at 37ºC for *E. coli* strains. M9 was used as minimal medium (Sambrook *et al.,* 1989) amended with different carbon sources at 0.2% (w/v). Unless otherwise indicated, the agar plates contained 1.5% (w/v) agar and were incubated overnight at 30ºC. For the colony morphology experiments, 2 µl of overnight cultures were spotted onto 1% (w/v) agar plates containing 10 g l^{-1} of tryptone and amended with 40 µg ml^{-1} Congo red and 20 µg ml^{-1} Coomassie brilliant blue, and incubated at RT for 24 h. To test polysaccharide production, 2 µl of overnight cultures were spotted onto LB agar plates containing 25 µg ml^{-1} calcofluor white and plates were incubated at 30ºC for 3, 5 and 7 days and observed under UV light. Phosphate-buffered saline (PBS; 8 mM Na_2HPO_4, 1.5 mM KH_2PO_4, 3 mM KCl, and 137 mM NaCl, pH 7) was used to wash or dilute cells. When required, the supplements were added at the following final concentrations: 500 µg ml^{-1} ampicillin (Ap) for *P. putida* and 150 µg ml^{-1} for *E. coli*; 50 µg ml^{-1} kanamycin (Km); 20 µg ml^{-1} gentamicin (Gm); 40 µg ml^{-1} 5-bromo-4-chloro-3-indolyl-β-D-galactopyranoside (Xgal); 1.0 mM isopropyl-β-D-1-thiogalactopyranoside (IPTG); and 15 mM 3-methyl-benzoate (3 MB). The growth kinetics of the two strains was determined according to the OD_{600} of the cultures in 96-well microtitre polystyrene plates (Nunc) using a SpectraMax M2^e plate reader (Molecular Devices). *In vitro* determinations of nucleotides were assessed using cells grown in shaken-flasks in M9 medium amended with 0.2% (w/v) glucose. For the phenotypic microarray comparison of the wild type and the Δflagella strains, we used the Phenotypic MicroArray™ (PM) platform (Bochner *et al.,* 2001; Bochner 2009). The complete analysis, using plates PM1 through PM20, was performed using Biolog Inc. (Hayward, CA, USA). This technology facilitates the performance of 1187 different physiological assays, including C, N, P and S utilisation and sensitivity to certain chemicals.

DNA techniques and generation of a flagella-deleted strain

The DNA was manipulated according to routine laboratory procedures as described in Sambrook *et al.,* (1989). Plasmid DNA was obtained using the Wizard Plus SV Miniprep kit (Promega). The PCR-amplified DNA was purified using the NucleoSpin Extract II (MN) kit. The complete set of primers used in this study is listed in Supplementary Table S3. To construct a strain devoid of the motility apparatus, we PCR amplified the region 750-bp upstream (TS1) and 816-bp downstream (TS2) of the PP4329 and PP4297 genes. Subsequently, both TS1 and TS2 fragments were ligated through SOEing-PCR (Horton *et al.,* 1989); the complete TS1-TS2 fragment was digested with EcoRI and BamHI and ligated into plasmid pEMG (Martinez-Garcia and de Lorenzo 2011) to generate plasmid pEMG-flagella. The plasmid was transformed into *E. coli* DH5$\alpha\lambda$*pir*, the positive clones were verified through DNA sequencing of the entire TS1-TS2 construct. Thus, the pEMG-flagella plasmid was mobilised to *P. putida* KT2440 (pSW-I) cells as previously described (Martinez-Garcia and de Lorenzo 2012). The positive co-integrates were selected through PCR amplification of the TS1-TS2 fragment, and resolved through induction of the I-SceI enzyme, derived from the pSW-I plasmid using 15 mM 3 MB. Subsequently, the induced culture was plated onto LB-Ap500 agar plates. The positive colonies were assessed for the loss of the Km resistance marker and PCR was performed to confirm the deletion. The pSW-I plasmid was cured after several passes of the deleted strain in LB without Ap500.

Morphological and physical tests

For electron microscopy, the bacterial cells were deposited onto thin carbon-coated collodion grids, negatively stained with 1% (w/v) uranyl acetate, and the images were obtained using a JEOL JEOM 1011 transmission electron microscope. To assess *motility*, the bacterial cells from overnight cultures were diluted to OD_{600} of 0.1 or 0.5 and 2 µl were spotted onto the surface of M9 minimal medium (Sambrook *et al.,* 1989) supplemented with 0.2% (w/v) of either succinate, glucose or fructose, and solidified with 0.3% (w/v) agar. The plates were incubated at 30ºC and the diameter of the swimming halo recorded at 48 h. For the *sedimentation assays*, bacterial strains were inoculated in 4 ml of LB and aerobically (170 rpm) cultured at 30ºC overnight. Thus, the OD_{600} of the cultures was measured, and this value was set to 100% (t = 0), then tubes were maintained still, without shaking, at RT for 24 h and a sample taken from the top part of the culture and the OD_{600} measured. To measure the *cell surface hydrophobicity* we used a previously described method (Rosenberg *et al.,* 1980; Rosenberg 1984).

Briefly, exponential cells were washed three times with phosphate-urea-magnesium sulphate buffer (PUM; 97 mM K_2HPO_4, 53.3 mM KH_2PO_4, 30 mM urea, 812 µM $MgSO_4$, pH 7.1), and the OD_{600} was adjusted to 0.6. Afterwards, 1.2 ml of the cell suspension was mixed with 0.2 ml of hexadecane, vortexed for 45 seconds, and the phases were equilibrated after incubating the tubes for 30 minutes at RT. Subsequently, the optical density of the aqueous phase measured and the microbial adherence to hydrocarbon (MATH) expressed as (1 - $OD_{final}/OD_{initial}$) x 100. To examine *biofilm formation,* the cells were grown aerobically (170 rpm) at 30ºC overnight. The OD_{600} of the cultures was adjusted to 0.05 before inoculating 200 µl into 96-well polystyrene plates (Nunc). The plates were incubated standing at room temperature for 5 h, 24 h or 4 days. Subsequently, a sample of the medium was removed and OD_{600} measured to estimate the planktonic cells in the culture. The plates were washed with water to remove all non-adhered cells, and stained with 0.1% (w/v) crystal violet for 30 minutes. The dye was removed and the plates were washed again with water, dried and the remaining stain dissolved with 33% (v/v) acetic acid. The absorbance was measured at 595 nm (biofilm formation). The biofilm index was calculated as the ratio of biofilm formation to planktonic cell density (biofilm formation /OD_{600}).

Determination of the ATP/ADP ratio, adenylate energy charge and redox ratios

The adenylate energy charge (AEC) is a quantitative measure of the relative saturation of high-energy phospho-anhydride bonds available in the adenylate pool (Chapman *et al.,* 1971; Barrette *et al.,* 1988) according to the following formula:

$$AEC = ([ATP]+0.5[ADP])/([ATP]+[ADP]+[AMP])$$

The AEC and ATP/ADP values were calculated according to the ATP, ADP and AMP content in deproteinised extracts from the strains under study. *In vitro* nucleotide determinations, based on an ATP bioluminescence assay, were conducted as previously described (Nikel and de Lorenzo 2013). The intracellular levels of pyridine nucleotide cofactors were estimated using *in vitro* cyclic assays, starting with the rapid inactivation of the metabolism of growing cells, followed by acid or alkaline nucleotide extraction, as previously described (Bernofsky and Swan 1973), with the modifications according to Nikel *et al.* (2008) and Chavarria *et al.* (2013). The intracellular concentration of the nucleotides was calculated as previously described (Fuhrer and Sauer 2009).

Stress resistance

For the liquid culture assays, the overnight cultures were diluted to an OD_{600} of 0.05 with and without the particular stressor and its growth was monitored according to the OD_{600} of the cultures in 96-well microtitre polystyrene plates for 24 h. The concentration of the stressors was adjusted to avoid the complete death of the cells. Paraquat was used at a final concentration of 10 µM for LB, M9 plus succinate, and M9 with glucose, and at 0.5 µM for fructose, while diamide was adjusted to 3 mM for LB, M9 plus succinate, and M9 with glucose, and 1.5 mM for fructose. The survival ratio was calculated as the OD_{600} with the drug *vs.* the OD_{600} without any added stressor through time. For the serial dilution experiments, the overnight bacterial cultures were diluted with PBS and 10 µl of each dilution from 10^{-2} to 10^{-9} was spotted onto LB agar plates amended with the stressor. The plates were incubated at 30ºC and photographed after 24 h. In the case of UV resistance, the OD_{600} of overnight cultures was adjusted to 0.1, and 30 µl of the resulting suspension was evenly distributed onto an LB agar plate, dried and irradiated with UV light (254 nm), with exposure times from 20 to 140 seconds. The plates were wrapped with aluminium foil to avoid photoreactivation and incubated at 30ºC for 20 h.

Flow cytometry

The appropriate liquid media was inoculated with bacteria from -80ºC frozen stocks, and the cultures were incubated overnight until saturation. LB cultures were diluted at 1/5 in phosphate-buffered saline (PBS; 8 mM Na_2HPO_4, 1.5 mM KH_2PO_4, 3 mM KCl, and 137 mM NaCl, pH 7.0), while M9 glucose cultures were not diluted. The cells were subsequently stained with PI at a final concentration of 1 µg ml^{-1} and analysed using a Gallios™ flow cytometer (Beckman Coulter Inc.) equipped with a laser of 22 mW at 488 nm as the excitation source. The fluorescence was recorded at 617 nm using a 620/30 nm bandpass filter. A total of 200,000 events were counted, and the percentage of PI-stained cells was determined.

Acknowledgements

Authors thank Carmen Moreno (CNB-CSIC) for technical assistance with the flow cytometry experiments and Cristina Patiño (CNB-CSIC) for help with the electron microscopy. This study was supported by the BIO and FEDER CONSOLIDER-INGENIO Program, the MICROME, ST-FLOW and ARISYS Contracts of the EU, the ERANET-IB program and the PROMT Project of the CAM. PIN is a researcher from the Consejo Nacional de Investigaciones Científicas y Técnicas (Argentina) and received a Marie Curie Actions Program grant from the EC (ALLEGRO, UE-FP7-PEOPLE-2011-IIF-300508). The authors declare that there are no conflicts of interest.

References

Ackermann M. 2008. Bacteria as a new model system for aging studies: investigations using light microscopy. *Biotechniques* **44**: 564-567.

Bagdasarian M, Lurz R, Ruckert B, Franklin FC, Bagdasarian MM, Frey J, Timmis KN. 1981. Specific-purpose plasmid cloning vectors. II. Broad host range, high copy number, RSF1010-derived vectors, and a host-vector system for gene cloning in *Pseudomonas*. *Gene* **16**: 237-247.

Barrette WC, Jr., Hannum DM, Wheeler WD, Hurst JK. 1988. Viability and metabolic capability are maintained by *Escherichia coli*, *Pseudomonas aeruginosa*, and *Streptococcus lactis* at very low adenylate energy charge. *J Bacteriol* **170**: 3655-3659.

Berg HC. 2003. The rotary motor of bacterial flagella. *Annu Rev Biochem* **72**: 19-54.

Bernofsky C, Swan M. 1973. An improved cycling assay for nicotinamide adenine dinucleotide. *Anal Biochem* **53**: 452-458.

Bibikov SI, Biran R, Rudd KE, Parkinson JS. 1997. A signal transducer for aerotaxis in *Escherichia coli*. *J Bacteriol* **179**: 4075-4079.

Blank LM, Ionidis G, Ebert BE, Buhler B, Schmid A. 2008. Metabolic response of *Pseudomonas putida* during redox biocatalysis in the presence of a second octanol phase. *FEBS J* **275**: 5173-5190.

Bochner BR. 2009. Global phenotypic characterization of bacteria. *FEMS Microbiol Rev* **33**: 191-205.

Bochner BR, Gadzinski P, Panomitros E. 2001. Phenotype microarrays for high-throughput phenotypic testing and assay of gene function. *Genome Res* **11**: 1246-1255.

Boyer HW, Roulland-dussoix D. 1969. A complementation analysis of the restriction and modification of DNA in *Escherichia coli*. *J Mol Biol* **41**: 459-472.

Bren A, Eisenbach M. 2000. How signals are heard during bacterial chemotaxis: protein-protein interactions in sensory signal propagation. *J Bacteriol* **182**: 6865-6873.

Bus JS, Gibson JE. 1984. Paraquat: model for oxidant-initiated toxicity. *Environ Health Perspect* **55**: 37-46.

Chapman AG, Fall L, Atkinson DE. 1971. Adenylate energy charge in *Escherichia coli* during growth and starvation. *J Bacteriol* **108**: 1072-1086.

Chavarria M, Kleijn RJ, Sauer U, Pfluger-Grau K, de Lorenzo V. 2012. Regulatory tasks of the phosphoenolpyruvate-phosphotransferase system of *Pseudomonas putida* in central carbon metabolism. *mBio* **3**.

Chavarria M, Nikel PI, Perez-Pantoja D, de Lorenzo V. 2013. The Entner-Doudoroff pathway empowers *Pseudomonas putida* KT2440 with a high tolerance to oxidative stress. *Environ Microbiol* **15**: 1772-1785.

Dalgaard P, Koutsoumanis K. 2001. Comparison of maximum specific growth rates and lag times estimated from absorbance and viable count data by different mathematical models. *J Microbiol Methods* **43**: 183-196.

Dasgupta N, Wolfgang MC, Goodman AL, Arora SK, Jyot J, Lory S, Ramphal R. 2003. A four-tiered transcriptional regulatory circuit controls flagellar biogenesis in *Pseudomonas aeruginosa*. *Mol Microbiol* **50**: 809-824.

del Castillo T, Ramos JL, Rodriguez-Herva JJ, Fuhrer T, Sauer U, Duque E. 2007. Convergent peripheral pathways catalyze initial glucose catabolism in *Pseudomonas putida*: genomic and flux analysis. *J Bacteriol* **189**: 5142-5152.

Dos Santos VA, Heim S, Moore ER, Stratz M, Timmis KN. 2004. Insights into the genomic basis of niche specificity of *Pseudomonas putida* KT2440. *Environ Microbiol* **6**: 1264-1286.

Fontaine F, Stewart EJ, Lindner AB, Taddei F. 2008. Mutations in two global regulators lower individual mortality in *Escherichia coli*. *Mol Microbiol* **67**: 2-14.

Friedman L, Kolter R. 2004. Genes involved in matrix formation in *Pseudomonas aeruginosa* PA14 biofilms. *Mol Microbiol* **51**: 675-690.

Fuhrer T, Sauer U. 2009. Different biochemical mechanisms ensure network-wide balancing of reducing equivalents in microbial metabolism. *J Bacteriol* **191**: 2112-2121.

Graf N, Altenbuchner J. 2011. Development of a method for markerless gene deletion in *Pseudomonas putida*. *Appl Environ Microbiol* **77**: 5549-5552.

1 Grant SG, Jessee J, Bloom FR, Hanahan D. 1990. Differential plasmid rescue from transgenic mouse
2 DNAs into *Escherichia coli* methylation-restriction mutants. *Proc Natl Acad Sci USA* **87**: 4645-
3 4649.
4 Hall-Stoodley L, Costerton JW, Stoodley P. 2004. Bacterial biofilms: from the natural environment to
5 infectious diseases. *Nat Rev Microbiol* **2**: 95-108.
6 Hansen SK, Haagensen JA, Gjermansen M, Jorgensen TM, Tolker-Nielsen T, Molin S. 2007.
7 Characterization of a *Pseudomonas putida* rough variant evolved in a mixed-species biofilm
8 with *Acinetobacter* sp. strain C6. *J Bacteriol* **189**: 4932-4943.
9 Harwood CS, Fosnaugh K, Dispensa M. 1989. Flagellation of *Pseudomonas putida* and analysis of its
10 motile behavior. *J Bacteriol* **171**: 4063-4066.
11 Hickman JW, Harwood CS. 2008. Identification of FleQ from *Pseudomonas aeruginosa* as a c-di-GMP-
12 responsive transcription factor. *Mol Microbiol* **69**: 376-389.
13 Horton RM, Hunt HD, Ho SN, Pullen JK, Pease LR. 1989. Engineering hybrid genes without the use of
14 restriction enzymes: gene splicing by overlap extension. *Gene* **77**: 61-68.
15 Imlay JA. 2013. The molecular mechanisms and physiological consequences of oxidative stress:
16 lessons from a model bacterium. *Nat Rev Microbiol* **11**: 443-454.
17 Jishage M, Ishihama A. 1997. Variation in RNA polymerase sigma subunit composition within different
18 stocks of *Escherichia coli* W3110. *J Bacteriol* **179**: 959-963.
19 Kessler B, de Lorenzo V, Timmis KN. 1992. A general system to integrate *lacZ* fusions into the
20 chromosomes of gram-negative eubacteria: regulation of the Pm promoter of the TOL plasmid
21 studied with all controlling elements in monocopy. *Mol Gen Genet:* **233**: 293-301.
22 Kirov SM. 2003. Bacteria that express lateral flagella enable dissection of the multifunctional roles of
23 flagella in pathogenesis. *FEMS Microbiol Lett* **224**: 151-159.
24 Kolter R, Greenberg EP. 2006. Microbial sciences: the superficial life of microbes. *Nature* **441**: 300-302.
25 Larsen SH, Adler J, Gargus JJ, Hogg RW. 1974. Chemomechanical coupling without ATP: the source of
26 energy for motility and chemotaxis in bacteria. *Proc Natl Acad Sci USA* **71**: 1239-1243.
27 Liu R, Ochman H. 2007. Stepwise formation of the bacterial flagellar system. *Proc Natl Acad Sci USA*
28 **104**: 7116-7121.
29 Lowe G, Meister M, Berg HC. 1987. Rapid rotation of flagellar bundles in swimming bacteria. *Nature*
30 **325**: 637-640.

Macnab R, (1996) Flagella and motility. In: *Escherichia coli* and *Salmonella*: Cellular and Molecular biology. F. C. Neidhardt, Curtis, R.III, Ingraham, J.L., Lin, E.C.C., Low, B.K., Magasanik, B., Reznikoff, W.S., Riley, M., Schaechter, M., Umbarger, H.E. (ed). Washington, DC: American Society of Microbiology, pp. 123-145.

Macnab RM. 1977. Bacterial flagella rotating in bundles: a study in helical geometry. *Proc Natl Acad Sci USA* **74**: 221-225.

Mailloux RJ, Lemire J, Appanna VD. 2011. Metabolic networks to combat oxidative stress in *Pseudomonas fluorescens*. *Antonie van Leeuwenhoek* **99**: 433-442.

Martinez-Garcia E, de Lorenzo V. 2011. Engineering multiple genomic deletions in Gram-negative bacteria: analysis of the multi-resistant antibiotic profile of *Pseudomonas putida* KT2440. *Environ Microbiol* **13**: 2702-2716.

Martinez-Garcia E, de Lorenzo V. 2012. Transposon-based and plasmid-based genetic tools for editing genomes of gram-negative bacteria. *Methods Mol Biol* **813**: 267-283.

Neidhardt FC, Ingraham JL, Schaechter M, (1990) Physiology of the Bacterial Cell: A Molecular Approach. Sinauer associates, Sunderland, MA.

Nelson KE, Weinel C, Paulsen IT, Dodson RJ, Hilbert H, Martins dos Santos VA, Fouts DE, Gill SR, Pop M, Holmes M, Brinkac L, Beanan M, DeBoy RT, Daugherty S, Kolonay J, Madupu R, Nelson W, White O, Peterson J, Khouri H, Hance I, Chris Lee P, Holtzapple E, Scanlan D, Tran K, Moazzez A, Utterback T, Rizzo M, Lee K, Kosack D, Moestl D, Wedler H, Lauber J, Stjepandic D, Hoheisel J, Straetz M, Heim S, Kiewitz C, Eisen JA, Timmis KN, Dusterhoft A, Tummler B , Fraser CM. 2002. Complete genome sequence and comparative analysis of the metabolically versatile *Pseudomonas putida* KT2440. *Environ Microbiol* **4**: 799-808.

Nikel PI. 2012. A brief guide to *Pseudomonas putida* as a microbial cell factory. http://goo.gl/DXF1y.

Nikel PI, de Lorenzo V. 2013. Engineering an anaerobic metabolic regime in *Pseudomonas putida* KT2440 for the anoxic biodegradation of 1,3-dichloroprop-1-ene. *Metab Eng* **15**: 98-112.

Nikel PI, Pettinari MJ, Ramirez MC, Galvagno MA, Mendez BS. 2008. *Escherichia coli arcA* mutants: metabolic profile characterization of microaerobic cultures using glycerol as a carbon source. *J Mol Microbiol Biotechnol* **15**: 48-54.

Pieper DH, Martins dos Santos VA, Golyshin PN. 2004. Genomic and mechanistic insights into the biodegradation of organic pollutants. *Curr Op Biotech* **15**: 215-224.

1 Poblete-Castro I, Becker J, Dohnt K, dos Santos VM, Wittmann C. 2012. Industrial biotechnology of
2 *Pseudomonas putida* and related species. *Appl Microbiol Biotechnol* **93**: 2279-2290.
3 Pratt LA, Kolter R. 1998. Genetic analysis of *Escherichia coli* biofilm formation: roles of flagella, motility,
4 chemotaxis and type I pili. *Mol Microbiol* **30**: 285-293.
5 Qian C, Wong CC, Swarup S, Chiam KH. 2013. Bacterial tethering analysis reveals a "run-reverse-turn"
6 mechanism for *Pseudomonas* spp. motility. *Appl Environ Microbiol* **79**: 4734-4743.
7 Rebbapragada A, Johnson MS, Harding GP, Zuccarelli AJ, Fletcher HM, Zhulin IB, Taylor BL. 1997.
8 The Aer protein and the serine chemoreceptor Tsr independently sense intracellular energy
9 levels and transduce oxygen, redox, and energy signals for *Escherichia coli* behavior. *Proc Natl*
10 *Acad Sci USA* **94**: 10541-10546.
11 Romling U, Bian Z, Hammar M, Sierralta WD, Normark S. 1998. Curli fibers are highly conserved
12 between *Salmonella typhimurium* and *Escherichia coli* with respect to operon structure and
13 regulation. *J Bacteriol* **180**: 722-731.
14 Rosenberg M. 1984. Bacterial adherence to hydrocarbons: a useful technique for studying cell surface
15 hydrophobicity. *FEMS Microbiol Lett* **22**: 289-295.
16 Rosenberg M, Gutnick D, Rosenberg E. 1980. Adherence of bacteria to hydrocarbons: A simple method
17 for measuring cell-surface hydrophobicity. *FEMS Microbiol Lett* **9**: 29-33.
18 Russell JB, Cook GM. 1995. Energetics of bacterial growth: balance of anabolic and catabolic reactions.
19 *Microbiol Rev* **59**: 48-62.
20 Sambrook J, Maniatis T, Fritsch EF, (1989) Molecular cloning a laboratory manual. Cold Spring Harbor
21 Laboratory Press, Cold Spring Harbor, N.Y.
22 Sauer K, Cullen MC, Rickard AH, Zeef LA, Davies DG, Gilbert P. 2004. Characterization of nutrient-
23 induced dispersion in *Pseudomonas aeruginosa* PAO1 biofilm. *J Bacteriol* **186**: 7312-7326.
24 Simm R, Morr M, Kader A, Nimtz M, Romling U. 2004. GGDEF and EAL domains inversely regulate
25 cyclic di-GMP levels and transition from sessility to motility. *Mol Microbiol* **53**: 1123-1134.
26 Toutain CM, Zegans ME, O'Toole GA. 2005. Evidence for two flagellar stators and their role in the
27 motility of *Pseudomonas aeruginosa*. *J Bacteriol* **187**: 771-777.
28 Wax R, Rosenberg E, Kosower NS, Kosower EM. 1970. Effect of the thiol-oxidizing agent diamide on
29 the growth of *Escherichia coli*. *J Bacteriol* **101**: 1092-1093.

Wei Y, Wang X, Liu J, Nememan I, Singh AH, Weiss H, Levin BR. 2011. The population dynamics of bacteria in physically structured habitats and the adaptive virtue of random motility. *Proc Natl Acad Sci USA* **108**: 4047-4052.

Williams SC, Hong Y, Danavall DCA, Howard-Jones MH, Gibson D, Frischer ME, Verity PG. 1998. Distinguishing between living and nonliving bacteria: Evaluation of the vital stain propidium iodide and its combined use with molecular probes in aquatic samples. *J Microbiol Methods* **32**: 225-236.

Wong S, Mekalanos JJ. 2000. Genetic footprinting with mariner-based transposition in *Pseudomonas aeruginosa*. *Proc Natl Acad Sci USA* **97**: 10191-10196.

1 **Table 1**. Bacteria and plasmids.
2

Strains	Description / relevant characteristics	Reference
E. coli		
DH5α	Cloning host; *supE44, ΔlacU169, (ϕ80 lacZ Δ M15), hsdR17, (rk^-mk^+), recA1, endA1, thi-1, gyrA, relA*	(Grant *et al.,* 1990)
DH5α*λpir*	Cloning host; *λpir* lysogen of DH5α	Lab collection
HB101	Helper strain; F^- λ^- *mcrB mrr hsdS20 recA13 leuB6 ara-14* Δ(*proBA*)*2 lacY1 galK2 xyl-5 mtl-1 rpsL20* (Sm^R), *glnV44*	(Boyer and Roulland-dussoix 1969)
P. putida		
KT2440	mt-2 derivative, cured of the TOL plasmid pWW0	(Bagdasarian *et al.,* 1981)
KT2440 Δflagella	KT2440 derivative, non-flagellated	This work
Plasmids		
pEMG	Km^R, *ori*R6K, *lacZα* with two flanking I-SceI sites	(Martinez-Garcia and de Lorenzo 2011)
pSW-I	Ap^R, *ori*RK2, *xylS*, P_m→*I-SceI*	(Wong and Mekalanos 2000)
pEMG-flagella	pEMG bearing a 1.56 kb TS1-TS2 EcoRI-BamHI insert for deleting the flagella operon	This work
pRK600	Cm^R; *ori*ColE1, RK2 mob^+, tra^+	(Kessler *et al.,* 1992)

3
4
5
6

FIGURES

Figure 1. Genetic organisation and deletion of the flagellar operon of *P. putida* KT2440.

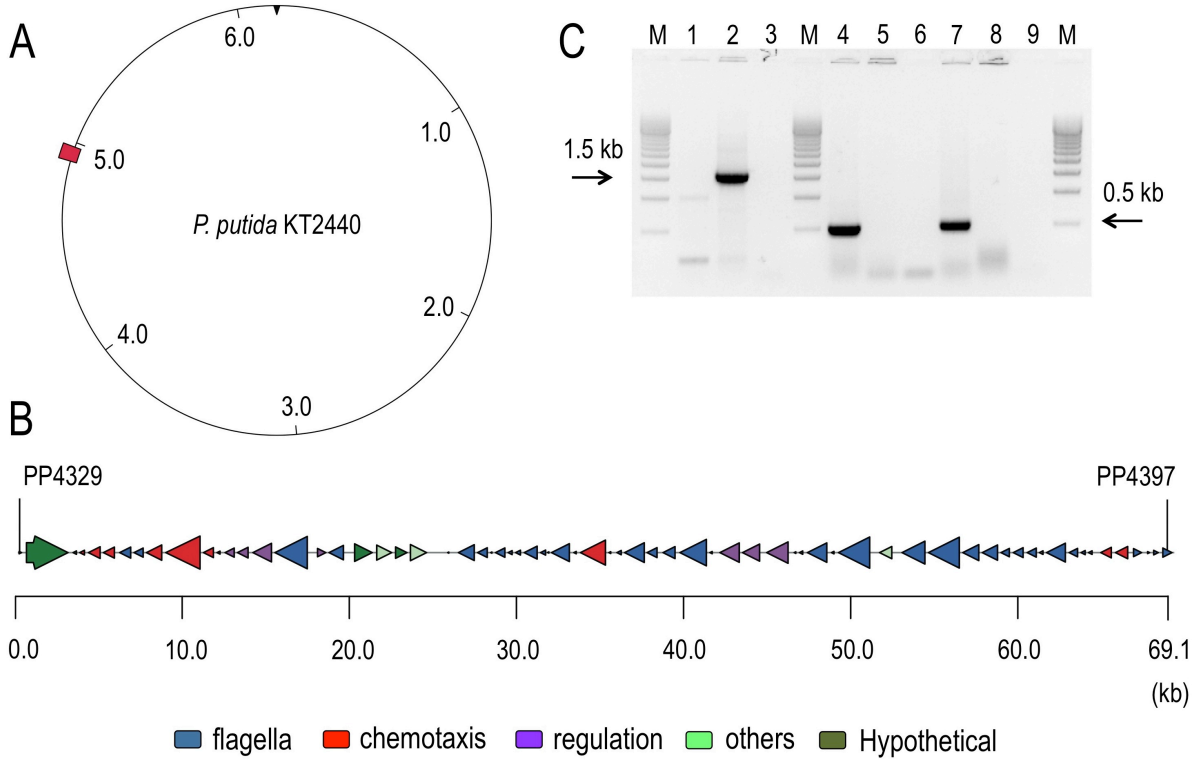

(**A)** Genomic map of *P. putida* KT2440 showing the physical localisation of the flagella operon within the chromosome. **(B)** The flagellar gene cluster. For a detailed description of the genes, see Supplementary Table S1. The functional classification of the genes was obtained from the *Pseudomonas* Genome Database (http://www.pseudomonas.com). The genes are represented as arrows and colour-coded according to their function. **(C)** Electrophoresis of the PCR analyses, confirming the deletion of the flagella operon. PCR analysis of the 1.5-kb TS1-TS2 fragment in the wild type (lane 1) and deleted strains (lane 2). Diagnostic amplification of the 0.5-kb sequence of the internal gene PP4335 of the flagellar operon in the wild type (lane 4) and deleted strains (lane 5). Analytical amplification of the 0.5-kb fragment of the internal gene PP4352 of the flagellar operon in the wild type (lane 7) and deleted strains (lane 8). M, the 500-bp Molecular ruler EZ load™ BioRad; lanes 3, 6 and 9 are negative controls with no DNA template.

Figure 2. Swimming tests and cell morphology of *P. putida* KT2440 with and without flagella.

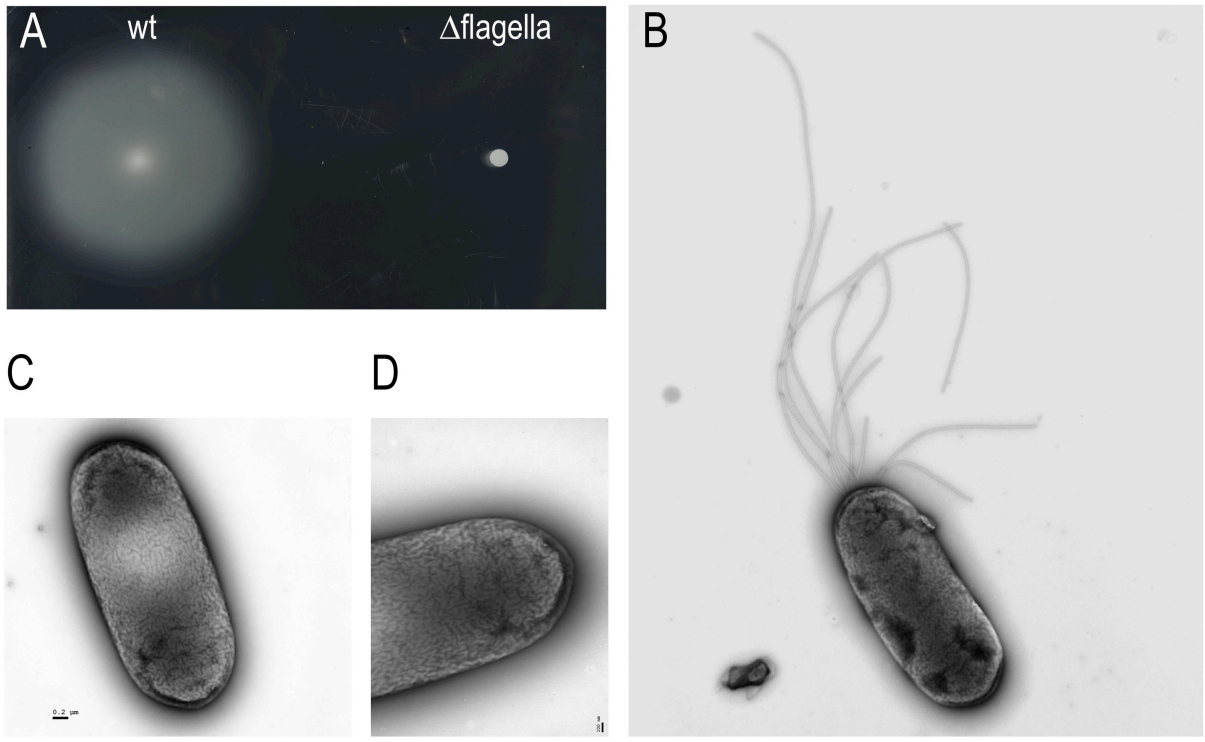

(A) Swimming halos. Aliquots of the wild type and non-flagellated cells were spotted on 0.3% (w/v) M9 agar plates supplemented with 0.2% (w/v) succinate and photographed at 48 h. **(B)** Electron microscopy images of wild type strain, note polar flagella. **(C, D)** A zoomed-in views of one of the poles of the non-flagellated strain The bacteria were negatively stained with 1% (w/v) uranyl acetate on thin-coated collodion grids. EM images were captured using a JEOL JEM 1011-transmission electron microscope operated at 100 kV.

Figure 3. Dispersion of flagella-less *P. putida* cells in liquid cultures**.**

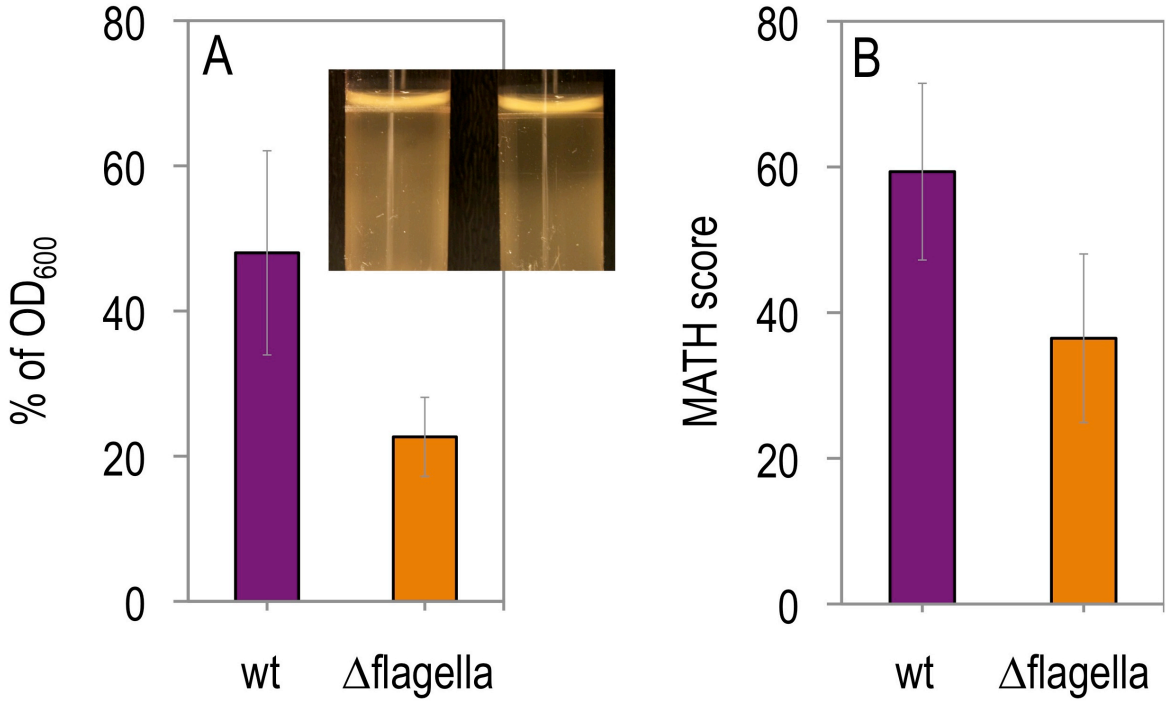

(A) Sedimentation assay of *P. putida* KT2440 and the non-flagellated strain. Saturated 4 ml LB liquid cultures (their OD_{600} was taken as 100%) were statically incubated at RT for 24 h, and the OD_{600} from the top part of the liquid culture was measured to estimate the sedimentation of each strain. The top right corner of a representative test tube is shown. The average and standard deviation of four independent experiments is shown. **(B)** Microbial Adhesion To Hydrocarbon (MATH) scores for the wild type and the non-flagellated strain. Exponentially-growing LB cultures were washed with PUM buffer and the adherence of the cells to hexadecane was determined. The MATH score is expressed as (1 - $OD_{final}/OD_{initial}$) x 100. The average and standard deviation of six independent experiments is shown.

Figure 4. Deletion of the flagella operon influences biofilm formation.

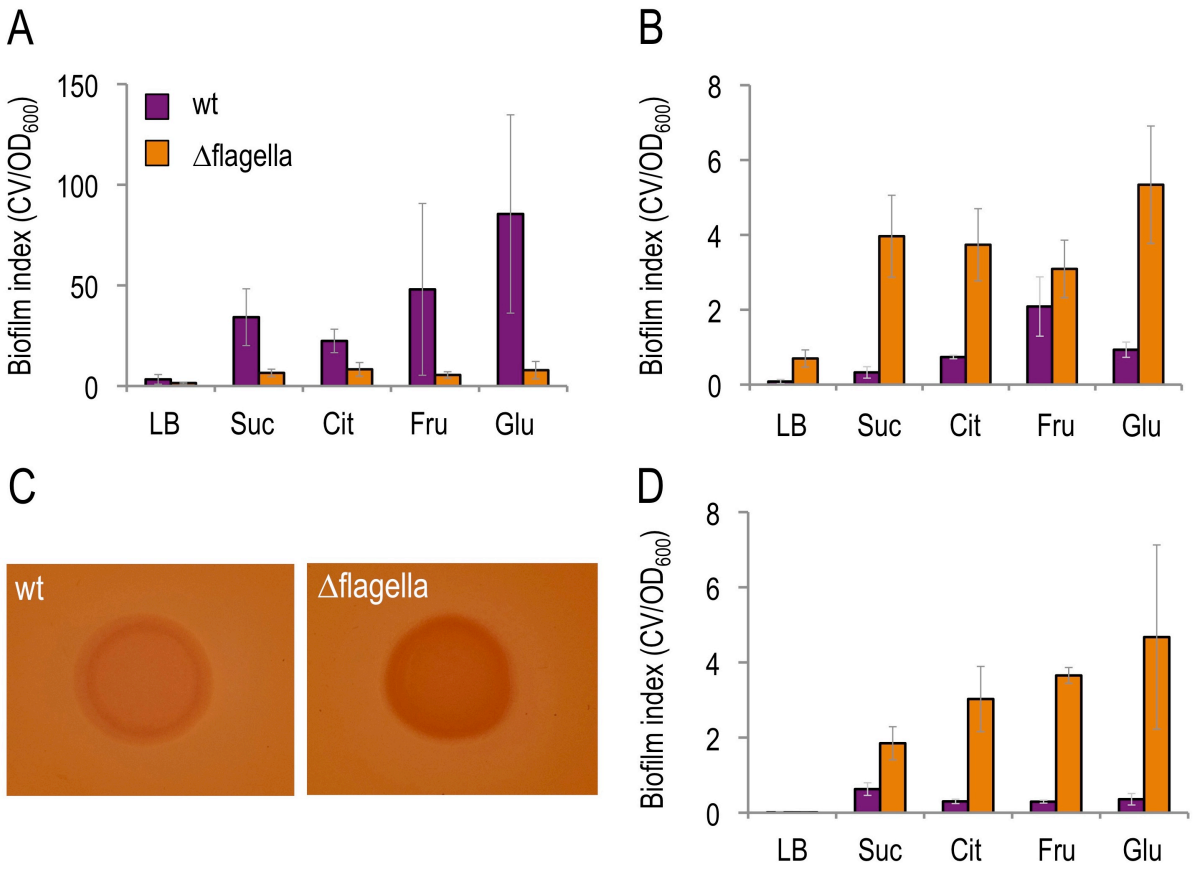

(**A)** Biofilm indexes after 5 h for the wild type (purple box) and non-flagellated strains (orange box) in different carbon sources: LB, M9+succinate (Suc), M9+citrate (Cit), M9+fructose (Fru), and M9+glucose (Glu). Biofilm formation was quantified using the crystal violet assay as described in Experimental procedures and the biofilm index calculated as the ratio of crystal violet (CV) staining (A_{595}) to planktonic cell density (CV/OD_{600}). **(B)** Same, after 24 h for the wild type (purple) and non-flagellated strains (orange) in different carbon sources: LB, M9+succinate (Suc), M9+citrate (Cit), M9+fructose (Fru), and M9+glucose (Glu). **(C)** Same, at 4 days for the wild type (purple) and non-flagellated strains (orange) in different carbon sources: LB, M9+succinate (Suc), M9+citrate (Cit), M9+fructose (Fru), and M9+glucose (Glu). The average of 3 biological experiments (with 8 technical replicates) is shown, and the error bars indicate standard deviations. **(D)** Cell growth morphology on tryptone agar plates with Congo red and Coomassie brilliant blue. 2 µl of an overnight culture were spotted onto the plates and incubated for 24 h at RT and photographed.

Figure 5. Growth curves for the *P. putida* KT2440 and the non-flagellated strain under different nutrient conditions.

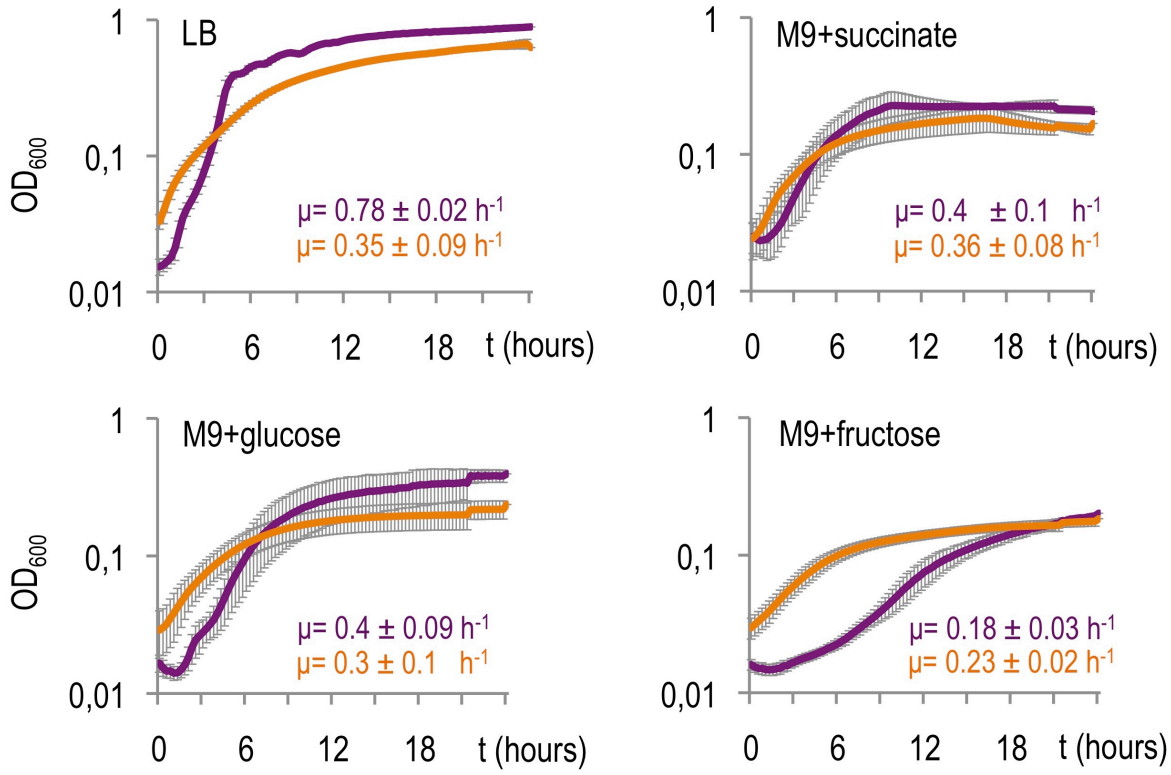

LB was used for a rich media and M9 was used for minimal media added with 0.2% (w/v) succinate, glucose, or fructose as the sole carbon source. The wild type strain is represented with a purple line, while the deleted strain is characterized with an orange line. The specific growth rates (μ) for the wild type (purple) and the non-flagellated (orange) strain are depicted within each chart. The experiment was performed using a plate reader with 96-well plates, and μ values were derived from the growth curves as described elsewhere (Neidhardt *et al.,* 1990; Dalgaard and Koutsoumanis 2001). The average and standard deviation of three independent experiments are shown.

Figure 6. Stress assays.

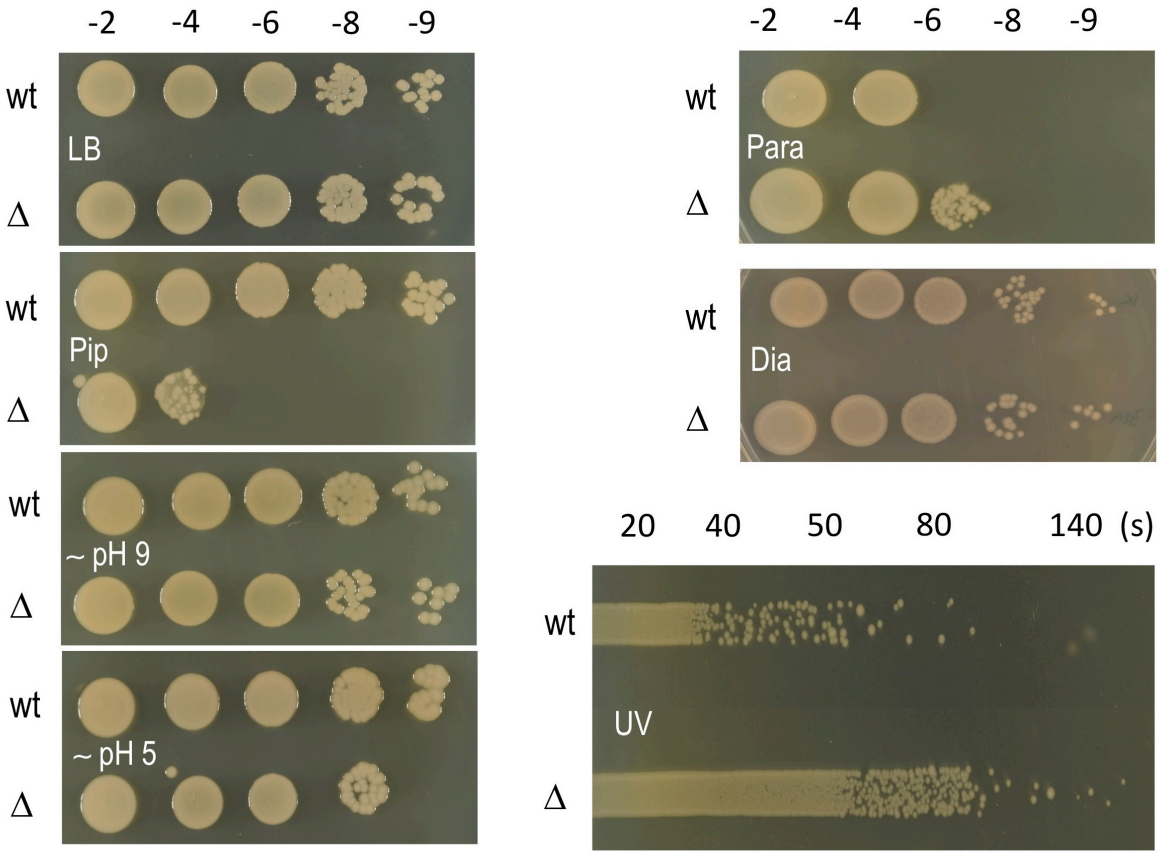

Serial dilution of overnight cultures placed on LB agar plates amended with different stressors. Pip, piperacillin; Dia, diamide; Para, paraquat. For the UV resistance, the cells were evenly spread onto an LB agar plate and irradiated with UV light for 20 to 140 seconds. The Δ symbol represents the non-flagellated strain.

Figure 7. Determination of energy and redox cofactors in *P. putida* KT2440 and its non-flagellated derivative.

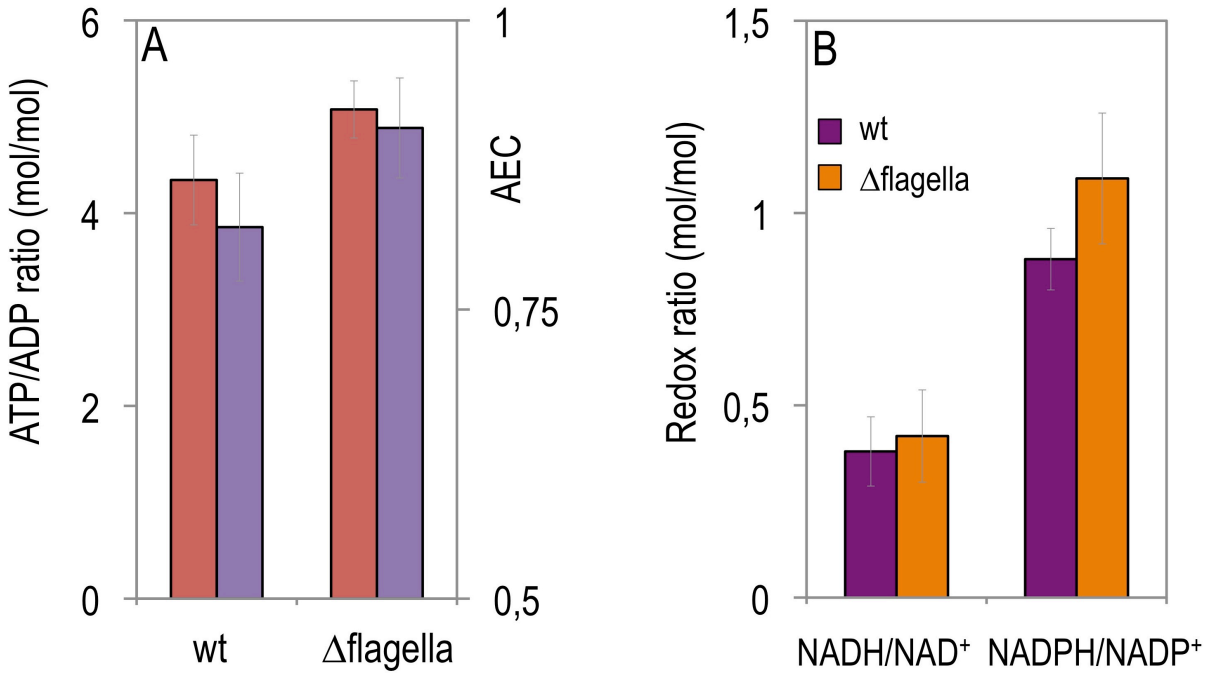

(A) ATP, ADP and AMP determinations were performed in exponentially-growing cells from M9 minimal medium cultures, containing 0.2% (w/v) glucose. Each bar represents the mean value ± standard deviation of the adenylate energy charge (AEC) (purple) or the ATP/ADP ratio (red) for duplicate measurements from at least three independent experiments. **(B)** Redox ratios were determined from the absolute intracellular concentrations of NAD^+, NADH, $NADP^+$, and NADPH. The pyridine nucleotide cofactors were enzymatically determined in exponentially-growing cells in M9 minimal medium containing 0.2% (w/v) glucose. In all cases, each bar represents the mean value ± standard deviation of the corresponding parameter for duplicate measurements from at least three independent experiments.

Figure 8. Stress resistance to paraquat and diamide in *P. putida* KT2440 and in the non-flagellated strain.

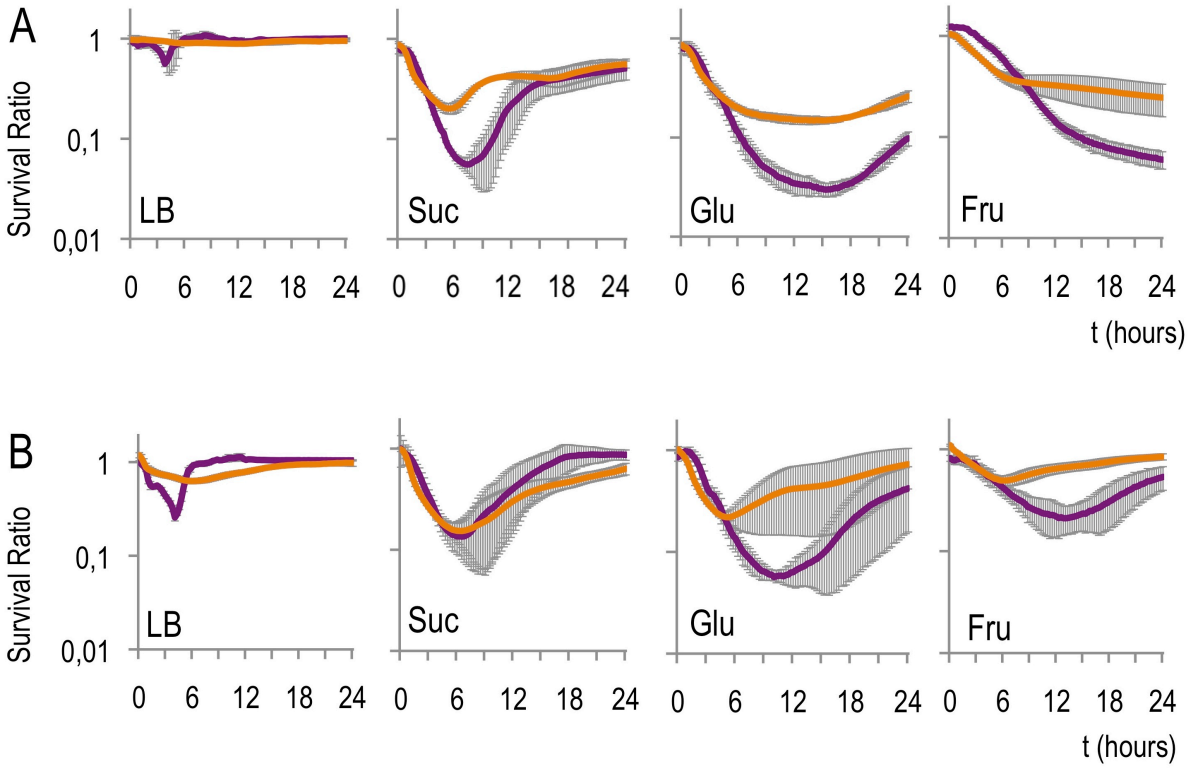

Survival ratios for wild type (purple) and non-flagellated cells (orange) exposed to paraquat (**A**) or diamide (**B**) in LB or M9 minimal medium with 0.2% (w/v) succinate (Suc) or fructose (Fru). The survival ratio was calculated as the OD_{600} after exposure to drugs divided by the OD_{600} before exposure to drugs. The experiments were performed using either 10 µM of paraquat for LB, M9 plus succinate, and M9 plus glucose, or 0.5 µM of paraquat for M9 plus fructose, and 3 mM diamide for LB, M9 plus succinate, and M9 plus glucose, or 1.5 mM diamide for M9 plus fructose. The average and standard deviation of three independent experiments is shown.

Figure 9. Cell mortality in stationary phase cultures.

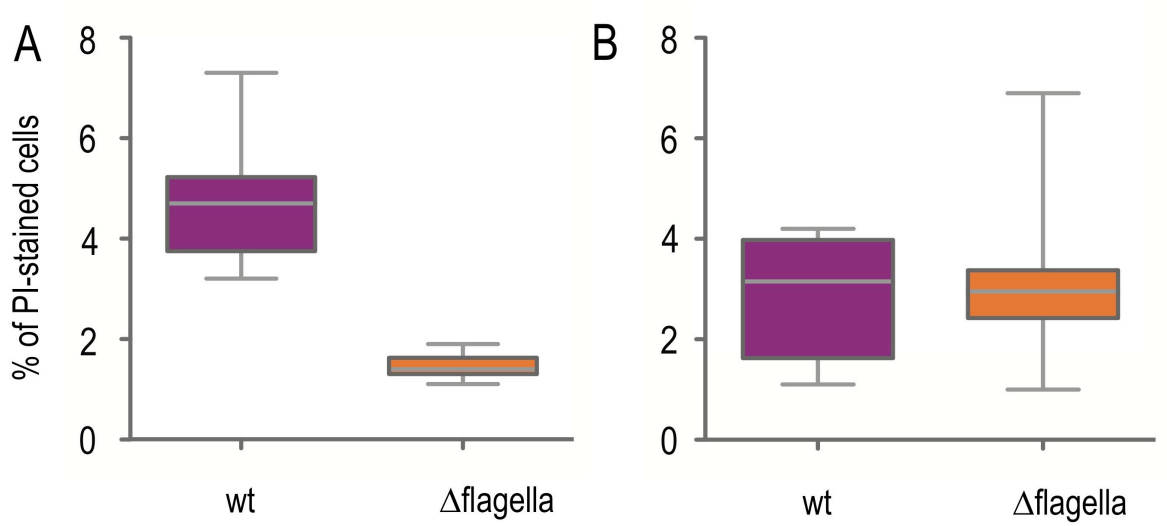

Cells grown overnight in LB (**A**) or M9 plus glucose (**B**) were stained with PI and the percentage of dead cells quantified through flow cytometry. The result of five independent experiments is represented in the box plot chart.

SUPPLEMENTARY INFORMATION

Supplementary Table S1. Flagellar operon genes grouped by its putative function.

Supplementary Table S2. Relevant phenotypes of the PM microarray analysis of the non-flagellated mutant compared to the wild-type strain.

Supplementary Table S3. Primers used in this study.

Supplementary Figure S1. Swimming patterns.

Supplementary Fig. S2. Consensus calls for the Biolog phenotypic microarray.

Supplementary Fig. S3. Stress resistance assays.

SUPPLEMENTARY INFORMATION

Supplementary Table S1. Flagellar operon genes grouped by its putative function (flagella synthesis and assembly, chemotaxis, regulation, other and hypothetical proteins of unknown function. Data retrieved from the *Pseudomonas* Genome Database (Winsor *et al.,* 2011)

Synthesis, assembly and export

[1]

PP#	Gene Name	Product Name
PP_4329		FlhB domain-containing protein
PP_4335	*motB*	flagellar motor protein MotD
PP_4336	*motC*	flagellar motor protein
PP_4344	*flhA*	flagellar biosynthesis protein FlhA
PP_4346	*ddlA*	D-alanine--D-alanine ligase A
PP_4351		FlhA-like protein
PP_4352	*flhB*	flagellar biosynthesis protein FlhB
PP_4353	*fliR*	flagellar biosynthesis protein FliR
PP_4354	*fliQ*	flagellar biosynthesis protein FliQ
PP_4355	*fliP*	flagellar biosynthesis protein FliP
PP_4356	*fliO*	flagellar assembly protein FliO
PP_4357	*fliN*	flagellar motor switch protein
PP_4358	*fliM*	flagellar motor switch protein FliM
PP_4359	*fliL*	flagellar basal body-associated protein FliL
PP_4361	*fliK*	flagellar hook-length control protein
PP_4365	*fliJ*	flagellar biosynthesis chaperone
PP_4366	*fliI*	flagellum-specific ATP synthase
PP_4367	*fliH*	flagellar assembly protein H
PP_4368	*fliG*	flagellar motor switch protein G
PP_4369	*fliF*	flagellar MS-ring protein
PP_4370	*fliE*	flagellar hook-basal body protein FliE
PP_4374		putative flagellar protein, FliT
PP_4375	*fliS*	flagellar protein FliS
PP_4376	*fliD*	flagellar cap protein FliD
PP_4377		flagellin FlaG, putative
PP_4378	*fliC*	flagellin FliC
PP_4380	*flgL*	flagellar hook-associated protein FlgL
PP_4381	*flgK*	flagellar hook-associated protein FlgK
PP_4382	*flgJ*	flagellar rod assembly protein/muramidase FlgJ
PP_4383	*flgI*	flagellar basal body P-ring protein
PP_4384	*flgH*	flagellar basal body L-ring protein
PP_4385	*flgG*	flagellar basal body rod protein FlgG
PP_4386	*flgF*	flagellar basal body rod protein FlgF
PP_4388	*flgE*	flagellar hook protein FlgE
PP_4389	*flgD*	flagellar basal body rod modification protein
PP_4390	*flgC*	flagellar basal body rod protein FlgC
PP_4391	*flgB*	flagellar basal body rod protein FlgB
PP_4394	*flgA*	flagellar basal body P-ring biosynthesis protein FlgA
PP_4396		FlgN family protein
PP_4397		type IV pilus assembly PilZ

Chemotaxis-related

PP#	Gene Name	Product Name
PP_4332	*cheW*	purine-binding chemotaxis protein CheW
PP_4333		CheW domain-containing protein
PP_4334		ParA family protein
PP_4337	*cheB*	chemotaxis-specific methylesterase
PP_4338	*cheA*	CheA signal transduction histidine kinase
PP_4339	*cheZ*	chemotaxis phosphatase, CheZ
PP_4340	*cheY*	response regulator receiver protein
PP_4362		Hpt protein
PP_4363		response regulator receiver protein
PP_4392	*cheR*	chemotaxis protein methyltransferase CheR
PP_4393	*cheV-3*	chemotaxis protein CheV

Regulation-related

PP#	Gene Name	Product Name
PP_4341	*fliA*	flagellar biosynthesis sigma factor
PP_4342	*fleN*	flagellar number regulator FleN
PP_4343	*flhF*	flagellar biosynthesis regulator FlhF
PP_4345		GntR family transcriptional regulator
PP_4364		anti-sigma F factor antagonist
PP_4371	*fleR*	two component, sigma54 specific, transcriptional regulator, Fis family
PP_4372	*fleS*	PAS/PAC sensor signal transduction histidine kinase
PP_4373	*fleQ*	sigma54 specific transcriptional regulator, Fis family
PP_4395	*flgM*	anti-sigma-28 factor, FlgM

Others

PP#	Gene Name	Product Name
PP_4348		cystathionine beta-lyase, putative
PP_4350		aminotransferase
PP_4379		beta-ketoacyl-acyl-carrier-protein synthase I

Hypothetical proteins

PP#	Gene Name	Product Name
PP_4330		hypothetical protein
PP_4331		hypothetical protein
PP_4347		hypothetical protein
PP_4349		hypothetical protein
PP_4360		hypothetical protein
PP_4387		hypothetical protein

Supplementary Table S2. Relevant phenotypes of the PM microarray analysis of the non-flagellated mutant compared to the wild type strain.

Plate Panel	Well(s)	Chemical	Category	Phenotype[a]
PM08	H08	Glycine-Phenylalanine-Phenylalanine	N-source (peptide)	+
PM01	A09	D-Alanine	C-source (aa)	–
PM01	G05	L-Alanine	C-source (aa)	–
PM02A	F06	Quinic acid	C-source	–
PM03B	C02	L-Valine	N-source (aa)	–
PM03B	B04	L-Isoleucine	N-source (aa)	–
PM06	G04	Isoleucine-Arginine	N-source (peptide)	–
PM08	E05	Tyrosine-Valine	N-source (peptide)	–
PM08	E04	Tyrosine-Isoleucine	N-source (peptide)	–
PM10	D12	pH 4.5 + Urea	pH (decarboxylase)	–
PM10	A03	pH 4.5	pH	–
PM10	A04	pH 5	pH	–
PM10	A05	pH 5.5	pH	–
PM11C	C05, C06, C07	Colistin	Membrane (cyclic peptide)	–
PM19	B02, B03, B04	Methyltrioctylammonium chloride	Membrane (cationic detergent)	–
PM15B	D06, D07	Domiphen bromide	Membrane (cationic detergent)	–
PM18C	C03	Poly-L-Lysine	Membrane (cationic detergent)	–
PM12B	C06, C07, C08	Vancomycin	Wall (antibiotic)	–
PM19	F02, F03	Phenethicillin	Wall (lactam)	–
PM11C	B07, B08	Cloxacillin	Wall (lactam)	–
PM19	A06, A07	Gallic acid	Respiration (ionophore, H^+)	–

Plate Panel	Well(s)	Chemical	Category	Phenotype[a]
PM19	C11, C12	Trans-Cinnamic acid	Respiration (ionophore, H^+)	−
PM11C	G10, G11	Potassium tellurite	Toxic anion	−
PM16A	F01, F02	Potassium tellurite	Toxic anion	−
PM20B	F02, F03	4-Hydroxycoumarin	DNA intercalator	−
PM20B	C05, C06, C07	Atropine	Acetylcholine receptor	−
PM20B	E05, E06, E07	n-Dodecylguanidine	Membrane permeability	−

a: (+) means that in that condition the mutant strain showed a higher respiration rate than the wt; (−) represents that the wt displayed a higher respiration rate than mutant cells.

Supplementary Table S3. Primers used in this study.

Name	Sequence 5' → 3'[a]	Usage
TS1-EcoRI-F	CG**GAATTC**CGAAGCGAAGCTGCTGAGTGGGTC	Deletion of flagella
TS1-R	*GCGTTTTCTGTTTTACCGACCGACGA*GCGGTTTCGTC CACCCAGCGTTG	Deletion of flagella
TS2-F	TCGTCGGTCGGTAAAACAGAAAACGC	Deletion of flagella
TS2-BamHI-R	CG**GGATCC**AGTACGGTGTTGGGCTCGGGGCT	Deletion of flagella
PP4335-F	TACCGAGGAACACGAAAACC	Diagnose deletion of flagella (PP4335)
PP4335-R	TTGGCAGGTTGTCAGTGAAG	Diagnose deletion of flagella (PP4335)
PP4352-F	GCGCATGAACTTCAGTTTGA	Diagnose deletion of flagella (PP4352)
PP4352-R	CCCTCGCTGTCCTTGTACTC	Diagnose deletion of flagella (PP4352)
Junction-F	CGCCAAGCCTCGCTACCCGGCCTGCT	Sequence boundaries of the Δflagella
Junction-R	CAGTTGATTCTGGTGGTGCACCCG	Sequence boundaries of the Δflagella
pSW-F	GGACGCTTCGCTGAAAACTA	Curation of pSW-I (Martinez-Garcia and de Lorenzo, 2011)
pSW-R	AACGTCGTGACTGGGAAAAC	Curation of pSW-I (Martinez-Garcia and de Lorenzo, 2011)

[a] Recognition site for the restriction enzymes specified are in bold in the DNA sequence

Supplementary Figure S1. Swimming patterns.

Fig. S1

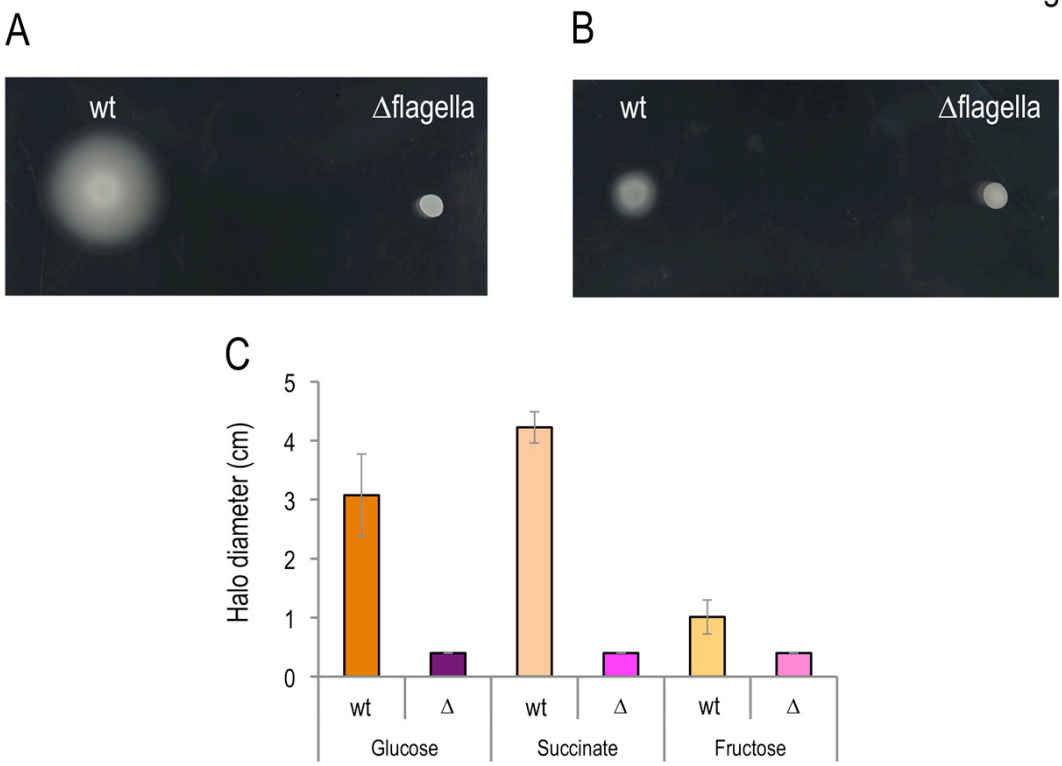

Aliquots of the wt and the deleted cells were spotted on 0.3% (w/v) M9 agar plates supplemented with 0.2% (w/v) glucose (**A**) or fructose (**B**) and photographed at 48 h. **C**: quantitative analyses of the swimming abilities of the wt and non-flagellated strains in M9 amended with glucose, succinate or fructose. The diameter of the swimming halos was recorded after 48 h of incubation at 30ºC. The Δ symbol represents the non-flagellated strain. The error bars represent the standard deviation.

Supplementary Fig. S2. Consensus calls for the Biolog phenotypic microarray.

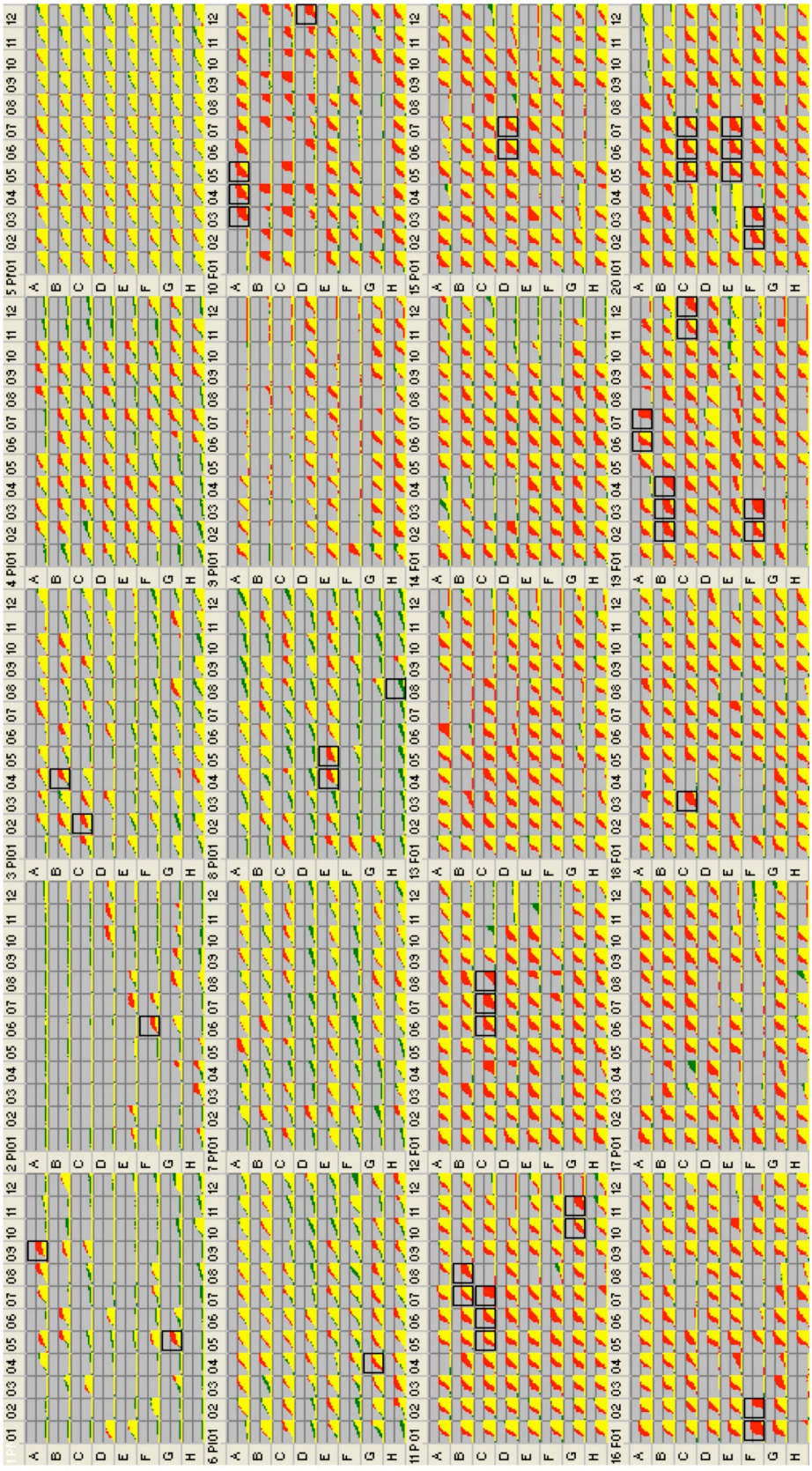

Yellow indicates that both strains, wt and mutant, have similar respiration levels. Red indicates a higher respiration of the wt, and green indicates when the mutant strain showed higher respiration. For the specific information about the different Biolog plates: http://www.biolog.com/pdf/pm_lit/PM1-PM10.pdf and http://www.biolog.com/pdf/pm_lit/PM11-PM20.pdf.

Supplementary Fig. S3. Stress resistance assays.

Fig. S3

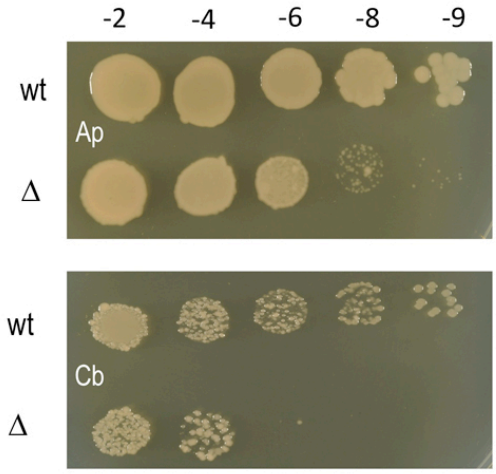

Serial dilution of overnight cultures placed on LB agar plates amended with Ap (ampicillin 50) or Cb (carbenicillin 250). The Δ symbol represents the non-flagellated strain.

References

Martinez-Garcia, E., and de Lorenzo, V. (2011) Engineering multiple genomic deletions in Gram-negative bacteria: analysis of the multi-resistant antibiotic profile of *Pseudomonas putida* KT2440. *Environ Microbiol* **13**: 2702-2716.

Winsor, G.L., Lam, D.K., Fleming, L., Lo, R., Whiteside, M.D., Yu, N.Y. et al. (2011) *Pseudomonas* Genome Database: improved comparative analysis and population genomics capability for *Pseudomonas* genomes. *Nucleic Acids Res* **39**: D596-600.